STATUS OF RESTRICTED SHOCK SEPRATION IN ROCKET NOZZLES

AFAQUE SHAMS & PIERRE COMTE

Laboratoire d'Etudes Aérodynamiques (LEA)
Université de Poitiers, ENSMA, CNRS

CEAT, 43 route de l'Aérodrome, F-86036 Poitiers, France

ABSTRACT

Appearance of restricted shock separated (RSS) flow depends upon the nozzle contour in a well defined range of nozzle pressure ratios (NPR). In spite of various experimental and numerical studies performed on this complicated separated flow, it is still not fully known. In the present study some light has been shed on various aspects of RSS flow regime. Three dimensional numerical simulations of thrust optimized contour (TOC) nozzle flow have been performed on wide range of nozzle pressure ratio (NPR), i.e. 25.0, 30.0, 38.0, 41.0 & 46.0. Detailed analysis of these numerical results allows examining the evolution of the separation point and the cap shock pattern with respect to the NPR. Furthermore, some insights based on the axial momentum along the nozzle axis and radial momentum distributions across the quadruple point are given.

1 AN OVERVIEW

Flow separation in rocket nozzles has been an area of interest over the last few decades. Several experimental, theoretical and numerical studies are performed to understand this separation phenomenon in rocket nozzles. Flow separation in rocket nozzles is considered undesirable due to its unsteady and non-symmetric nature which causes dangerous lateral forces, known as side-loads. These side-loads may cause structural damage. Extensive investigations of flow separation in conical rocket nozzles, running under over-expanded condition, were performed at the JPL during the late 1940s and early 1950s [1]. It was reported that when nozzle wall pressure at the nozzle exit was lowered by more than about 0.4 times the ambient pressure, flow separation takes place. Due to this separation wall pressure quickly rises to a plateau (slightly lower than the ambient pressure). This sudden rise in wall pressure is because of the separation shock formed by the strong change in pressure. Once the flow was separated, no reattachment occurred: that is why this type of flow separation is known as "free shock separation" (FSS).

Later on in 1973, the work of Nave and Coffey [2] on the J-2S engine demonstrated that apart from FSS flow regime there exists another type of flow separation, known as "Restricted Shock Separation" (RSS). This special flow is characterized by a small recirculation pocket followed by reattachment of separated flow back on the nozzle

wall. The main flow involves a special shock pattern called cap-shock followed by a trapped vortex surrounded by an annular supersonic jet.

Restricted shock separation is a complex flow regime, and a number of experimental and numerical studies in the past have been performed to understand the phenomenology of the flow [2]-[18]. RSS flow regime was observed only in thrust optimized contour (TOC) [2] and, more recently, in compressed truncated perfect (CTP) nozzles [15], i.e. in nozzles involving an internal shock in the full flowing regime. Restricted shock separated flow is characterized by a small recirculation pocket followed by reattachment on the nozzle wall. The main flow involves a special shock pattern called cap-shock followed by a trapped vortex surrounded by an annular supersonic jet. Existence of reversed flow (trapped vortex) in the plume of these nozzles, which was first reported by Chen et al. [3], has been confirmed by several numerical [14], [18] and experimental [8] investigations. It is believed that this trapped vortex is linked with the cap-shock pattern. With axi-symmetric RANS calculations on a TOC nozzle, Frey and Hagemann [6] have shown that this cap-shock can be interpreted as the inverse Mach reflection of the internal shock, which emanates from the region close to the nozzle throat. A 3D unsteady numerical simulation of the flow in a TOC nozzle has been performed by Deck et al. [11]& [14], but their study was mainly devoted to the hysteresis of the transition between the FSS and RSS regimes and to the evaluation of side-loads. Shimizu et al. [15] investigated flow transition from FSS to RSS in a CTP nozzle. In the RSS flow regime they were not able to detect the weak internal shock which interacts with the Mach disk but observed a small low-expansion region attached to the Mach disk.

In this paper a detailed study of RSS flow regime has been carried out. For that reason 3D numerical investigations are performed on a thrust optimized contoured (TOC) nozzle, investigated at Laboratoire d'Etudes Aérodynamiques (LEA), France [19], and is denoted as LEATOC nozzle. The following points have been studied and discussed in detail:

- Phenomenology of restricted shock separation and cap-shock pattern which is the main cause for RSS.
- Visualisation of flow discontinuities with the help of shock and compression functions [15], [20].
- Behaviour of internal shock (that appears near the throat of the nozzle) at different nozzle pressure ratios (NPR).
- Length of the cap-shaped oblique shock with respect to the separated incident oblique shock with the variation of the NPR.
- Size and behaviour of the trapped vortex that appears behind the cap-shock pattern and its 3D effects.
- How the size of the recirculation bubble (that appears due to the reattachment of the separated flow) vary with the NPR.

Detached-Eddy Simulation [18] of RSS flow regime at a wide range of NPR (i.e. 25.0, 30.0, 38.0, 41.0 and 46.0) have been performed to investigate and answer the aforementioned points in detail.

2 NUMERICAL METHODS & TURBULENCE MODELLING

Numerical simulations are performed on a thrust optimized contour nozzle by using the code TGNS3D developed at CEAT/LEA (Poitiers, France). This code solves the three dimensional unsteady compressible Navier-Stokes equations on multiblock structured grid.

The Navier-Stokes equations are discretized in space by using a cell centered finite volume method. A fifth order monotonicity preserving weighted essentially non-oscillatory (MPWENO) numerical scheme is used to achieve high accuracy results in such a complex flow where low order dissipative schemes are not efficient enough.

A second order implicit scheme has been implemented for time discretization. A diagonally dominant alternating direction implicit (DDADI) approach has been used for the inversion of the large sparse matrix system resulting from the implicit scheme.

All simulations are performed by using newly proposed DES by Shams et al. [18]. This DES approach has shown results in good agreement with the experimental data, for shock-separated flows in rocket nozzles.

3 FLOW PHYSICS

In rocket nozzles with conical and thrust optimized (TO) contours, an internal shock is generated near the throat region. In parabolic and thrust optimized contour nozzles this internal shock interacts with the small normal shock far away from the throat. A triple point exists, where the internal shock, the Mach stem and the cone-shaped oblique shock meet, indicating a connection between the internal shock and the existence of a cap-shock pattern which is responsible for the flow reattachment (Fig. 1).

In conical nozzles, although there exists an internal shock, these various internal shock reflections at the centerline destroy the high Mach number flow, and the Kernel is closed shortly downstream of the throat. Therefore, we do not see any cap-shock pattern nor reattachment of the flow . In contrast, in Truncated Ideal Contoured (TIC) nozzles, no such internal shock exists and we see only free shock separated flows in TIC types nozzle. In the recent past, the appearance of restricted shock separated flow has been reported in a Compressed Truncated Perfect Nozzle [15]. However they were unable to detect the internal shock due to the pattern of iso-Mach contours but have reported some low expansion region near the Mach reflection and suddenly the inverse Mach reflection is seen.

From the above discussion one can conclude that this reattachment of the separated flow depends on the nozzle contour in a defined range of NPR. Figure 1 shows the restricted shock separated flow regime. A large stabilized trapped vortex downstream of the cap-shock pattern is shown with the help of Q-criterion coloured with momentum in the x-direction and streamlines. As depicted from Fig. 1, RSS flow regime exhibits a number of flow discontinuities which are a bit difficult to differentiate or even detect (e.g. internal shock) with iso-Mach contours. Therefore we have used the following shock function [20], defined by:

$$f(x) \equiv \frac{\mathbf{U}}{c} . \frac{\texttt{grad}\, p}{|\texttt{grad}\, p|} \tag{1}$$

Figure 2, shows the iso-contours of shock function and one can see the clear vision of flow discontinuities, internal shock, cap-shock triple and quadruple points etc. Dark

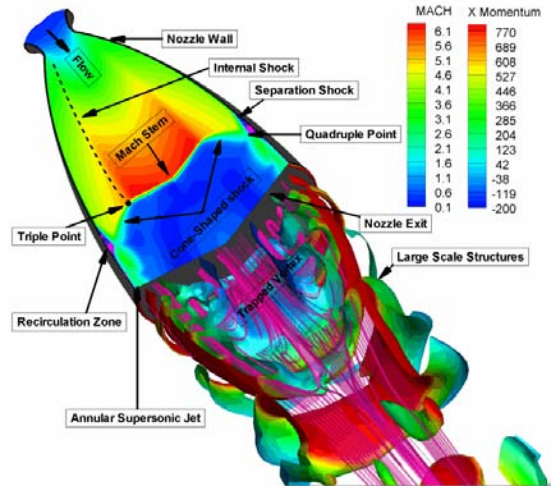

Figure 1: Restricted shock separation flow regime.

regions (negative value of the shock function) indicates the expansion in the flow and bright (positive value) zones highlight the compression regions. The annular supersonic jet which reattaches back to the nozzle wall exhibits successive interactions of shock and expansion waves, which sometimes leads to secondary flow separation which is shown in the following section. For more details about RSS flow regime see [18].

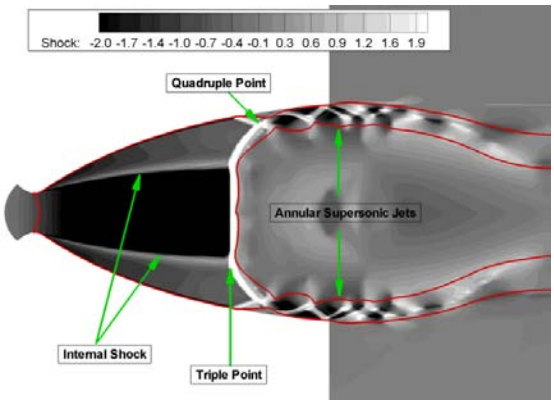

Figure 2: Iso-contours of shock function (f(x)).

4 EVOLUTION OF WALL PRESSURE

Evolution of mean wall pressure in the case RSS flow regime is quite complicated due to the reattachment of the supersonic jet. To understand the pressure evolution along the nozzle wall, mean wall pressure at two NPRs is shown in Fig. 3, along with the experimental data, and shows an excellent agreement.

The adverse pressure gradient causes the boundary layer to separate and the subsequent formation of a separation shock causes sudden increase in the wall pressure.

When the separated supersonic jet reattaches back to the nozzle wall, it makes the pressure increase even higher than the ambient pressure. The annular supersonic flow is subjected to expansion and compression waves reflected between the nozzle wall and the mixing layer separating the high speed region from the central trapped vortex. These reflected waves give an oscillatory wall pressure distribution which can lead in some case to secondary separation shown by Nguyen [12].

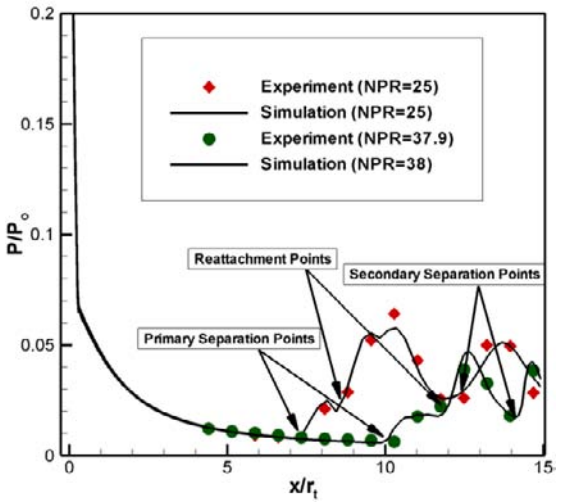

Figure 3: Evolution of mean wall pressure.

5 SEPARATION POINT & MACH STEM LOCATION

Increase in nozzle pressure ratio causes the separation point and corresponding Mach stem to move further downstream (towards the nozzle exit), whatever the flow configuration is, FSS or RSS. In the case of FSS flow regimes the respective distance between the separation point and Mach stem remains almost constant. Whereas, in RSS flow regime this is not the case, although at the initial stages (say NPR $\geq$ 24, when flow is in RSS zone) the respective distance between separation point and the Mach stem is quite small as compared to the FSS regime. Table 1 shows the numerically observed positions of the separation point, Mach stem and their respective quadruple point along with their corresponding NPRs.

NPR	$(\Delta X/r_t)_{MS-SP}$	$(\Delta X/r_t)_{QP-MS}$
25.0	0.90	1.13
30.0	0.57	1.15
38.0	-0.11	1.18
41.0	-0.20	1.96
46.0	-0.47	2.23

Table 1: Separation point (SP), Mach stem (MS) and quadruple point (QP) locations against their corresponding NPR

One can notice that for NPR=25.0, relative difference between Mach stem and separation point locations is positive, which is equal to 0.9 times the throat radius. This suggests that the Mach stem is located downstream of the separation point location. With the increasing NPR (say for 30.0) this difference decreases and even becomes negative for NPR=38.0. This means that the movement of the separation point location with respect to the Mach stem increases for higher NPR (i.e. 41.0, 46.0).

6 BEHAVIOUR OF RECIRCULATION ZONES

Apparently two different recirculation zones appear in RSS flow regime (i) a recirculation bubble, which is trapped between separation and reattachment of supersonic jet and (ii) a trapped vortex, large stabilized adverse pressure recirculation zone behind the cap-shock pattern.

Based on unsteady flow behaviour minimum and maximum ranges of these recirculation zones are given in Tables 2 & 3 respectively, against their corresponding NPRs. The overall range of the recirculation bubble varies from 1.69 to 2.33 times the nozzle throat radius. The size of these recirculation zones is directly linked with the separation and reattachment point locations. It is shown in the previous section that the respective difference between separation and reattachment point locations increase with the increase in NPR, also depicted from results in Table. 2.

NPR	Minimum Range ($\Delta X/r_t$)	Maximum Range ($\Delta X/r_t$)
25.0	1.69	1.97
30.0	2.03	2.17
38.0	2.16	2.29
41.0	2.19	2.30
46.0	2.24	2.33

Table 2: Evolution of minimum and maximum range of recirculation bubble with the increase in NPR

The same kind of interpretation holds for the stabilized trapped vortex which appears just downstream of the cap-shock. The respective movement of Mach stem towards the nozzle exit with the increase in NPR causes an increase in the size of the trapped vortex, ranging from 1.32 (minimum) to 1.65 (maximum) times the nozzle exit radius. The difference between the minimum and maximum range of this trapped vortex shows an increase for higher NPR, which shows that for higher NPR a high level of fluctuations appears.

7 BEHAVIOUR OF AXIAL & RADIAL MOMENTUM

In RSS flow regime, an internal shock from the throat region interacts with the Mach and forms a triple point with a cone-shaped shock (see Fig. 1). A slip line emanates from this triple point, which is inclined away from the nozzle axis and diverts the flow towards the nozzle wall due to the increasing radial momentum. To understand this phenomenon, radial momentum profiles (from nozzle axis to wall) before and after Mach stem are shown in Fig. 4.

NPR	Minimum Range ($\Delta X/D_e$)	Maximum Range ($\Delta X/D_e$)
25.0	1.32	1.48
30.0	1.33	1.51
38.0	1.34	1.53
41.0	1.38	1.61
46.0	1.41	1.65

Table 3: Evolution of minimum and maximum range of trapped vortex with the increase in NPR

The upstream location (before the Mach stem) for radial momentum distribution w.r.t the Mach stem (MS) is $\frac{\Delta x}{r_t} = 0.6$. The downstream position is selected as the quadruple point location observed against the mentioned NPRs. Radial momentum distribution before the Mach stem shows the positive value because of the expansion region. Downstream of the Mach stem, value of radial momentum increases slowly from zero (nozzle axis) on the positive side. Near the triple point region it shows a sudden increase in the value of radial momentum and reaches its maximum at the quadruple point. Above the quadruple point radial momentum decreases and turns into negative zone (momentum towards nozzle axis) caused by a small recirculation zone, and finally falls at the wall. The range of the radial momentum on the both positive and negative side increases with the increase in the NPR. This is due to the fact that relative size of recirculation bubble and cone-shaped shock increase for higher NPR.

With this increase in positive radial momentum downstream of Mach stem, pressure along the nozzle axis increases and produces a negative force against the main flow. This negative force in terms of axial momentum along the nozzle is shown in Fig. 5. Axial momentum and Mach number distribution seems to be the good detector for the size of the trapped vortex (also shown in Table. 3). Figure 5 shows that the minimum values of Mach number correspond to the locations where axial momentum turns from positive to negative values, indicating the range of the trapped zone.

Increase in the NPR (chamber pressure) causes the movement of cap-shock pattern towards the nozzle exit. The position of the Mach stem is determined by a balance between the positive axial momentum just downstream of the Mach stem (before the stagnation point) and a negative axial momentum in the trapped vortex (after the stagnation point). Whereas in the outer part of cap-shock pattern we have large amount of positive axial momentum corresponding to the supersonic flow regime. The position of the separation point is determined by the level of pressure in the recirculation bubble. As we have seen the difference between the locations of Mach stem and the separation point along the nozzle axis goes from positive to negative. As a consequence of this movement, the length of the cone-shaped shock relatively increases whereas the length of the separation shock decreases. The resulting radial momentum away from the nozzle axis relatively increases.

8 CONCLUSIONS

Three dimensional numerical investigation of restricted shock separated flow has been done on thrust optimized contour, LEATOC, nozzle. In LEATOC nozzle appearance of RSS flow regime starts for NPR ≥ 24. Simulations are performed at five different NPRs starting from 25.0 to 46.0. With the increase in NPR (in RSS range) separation point

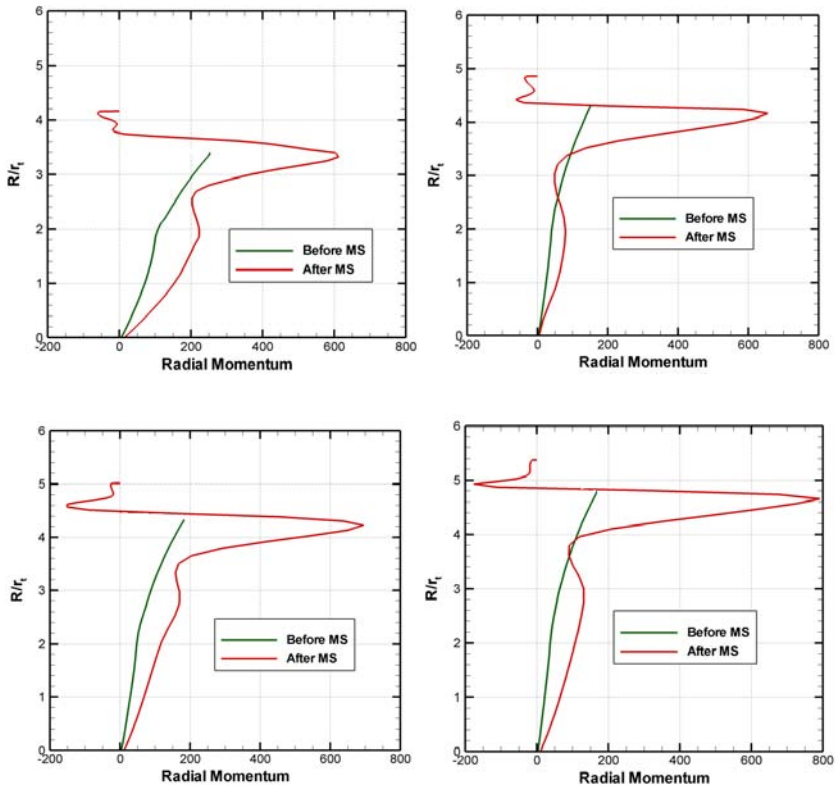

Figure 4: Distribution of radial momentum before and after Mach steam for NPR = 25.0 (a), 38.0 (b), 41.0 (c) & 46.0 (d).

locations move from upstream to downstream of the Mach stem. As a consequence, the size of the cone-shaped shock increases. This movement of separation point location also causes the increase in the size of recirculation zone trapped between the separation and reattachment of the annular supersonic jet. On the other hand relative size of the stabilized trapped vortex downstream of the cap-shock pattern increases by varying the NPR in the ascending order. Negative axial momentum distribution along the nozzle axis downstream of the cap-shock pattern produces a push against the main flow, and is one of the possible sources due to which separation point locations shift downstream of the Mach stem. Radial momentum distribution across the respective quadruple points shows increase with the increase in NPR, this also justifies the above mentioned argument.

ACKNOWLEDGEMENT

The Higher Education Commission (HEC), Government of Pakistan, is acknowledged for the research grant. The first author would like to thank T. Alziary de Roquefort for many discussions related to this research work.

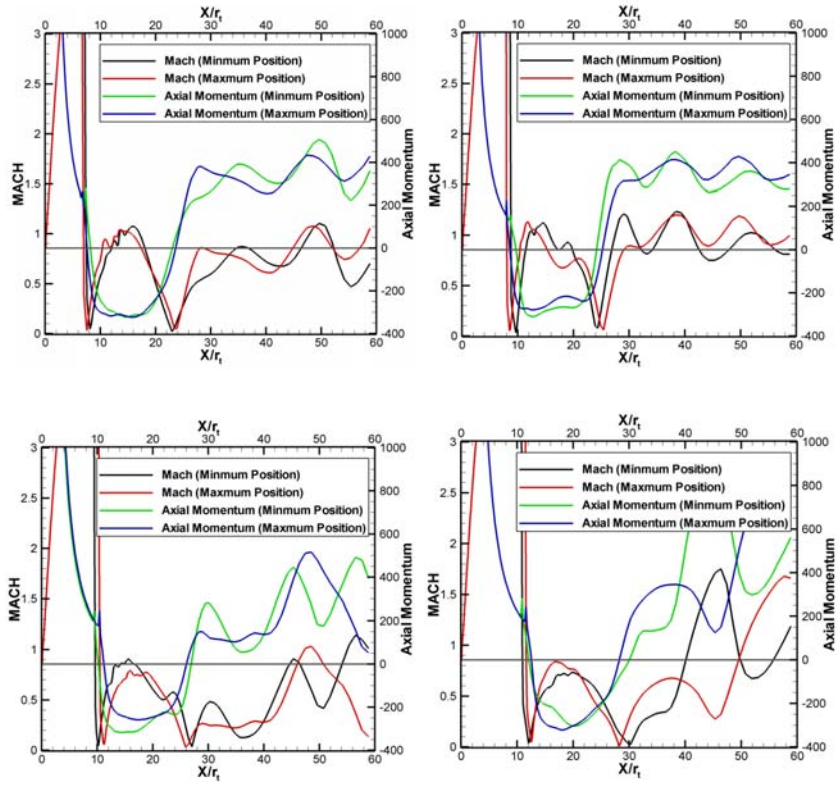

Figure 5: Evolution of axial momentum along the nozzle axis for NPR = 25.0 (a), 38.0 (b), 41.0 (c) & 46.0 (d).

References

[1] M. Summerfield, C. Foster & W. Swan, 1954, Flow separation in overexpanded supersonic exhaust nozzles, Jet Propulsion, pp. 319 ff., September-October.

[2] L. H. Nave & G. A. Coffey, 1973, Sea level side loads in high-area-ratio rocket engines, AIAA Paper 73-1284.

[3] C. L. Chen, S. R. Chakravarthy & C; M. Hung, 1994, Numerical investigation of separated nozzle flow, AIAA J. 32 (9) 1836-1843.

[4] M. Frey & G. Hagemann, 1998, Status of flow separation prediction in rocket nozzles, AIAA Paper 98-3619.

[5] M. Frey & G. Hagemann, 1999, Flow separation and side-loads in rocket nozzles, AIAA Paper 99-2815.

[6] M. Frey& G. Hagemann, 2000, Restricted Shock Separation in rocket nozzles. Journal of Propulsion and Power, Volume 16, No. 3, May-June.

[7] G. Hagemann, M. Frey & W. Koschel, 2002, Appearance of restricted shock separation in rocket nozzles. Journal of Propulsion and Power, Volume 18, No. 3, May-June.

[8] P. Reijasse, F. Bouvier & P. Servel, 2002, Experimental and numerical investigation of the cap-shock structure in over-expanded thrust-optimized nozzles. West-East High Speed Flow Field Conference Marseille, France.

[9] C. Pilinski, 2002, Etude numérique du décollement en tuyére supersonique. PhD Thesis, INSA de Rouen.

[10] S. Deck, 2002, Simulation Numérique des charges latérales instationaires sur des configuration de lanceurs. PhD Thesis, Université d'Orléans.

[11] S. Deck, E. Garnier & P. Guillen, 2002, Turbulence modelling applied to space launcher configurations. Journal of Turbulence, 3, 057.

[12] A.T. Nguyen, 2003, Ecoulement instationaire et charges latérales dans les tuyéres propulsives. PhD Thesis, Université de Poitiers.

[13] A. T. Nguyen, H. Deniau, S. Girard & T. Alziary de Roquefort, 2003, Unsteadiness of flow separation and end-effects regime in a thrust-optimized contour rocket nozzle. Flow, Turbulence and Combustion, 71: 161-181, 2003.

[14] S. Deck & A. T. Nguyen, 2004, Unsteady side loads in a thrust-optimized contour nozzle at hysteresis regime, J. Propulsion and Power 42 (9) 1878-1888.

[15] T. Shimizu, M. Hiroshi & K. Masatoshi, 2006, Numerical study of restricted shock separation in a compressed truncated perfect nozzle. AIAA Journal Vol. 44, No. 3.

[16] G; Hagemann & M. Frey, 2008, Shock pattern in the plume of rocket nozzles: needs for design consideration. Shock Waves, 17: 387-395.

[17] A. M. José & J. S. José, 2008, Numerical study of the start-up process in an optimized rocket nozzle, Aerospace Sci. & Tech., 12 (2008) 485-489.

[18] A. Shams, P. Comte, S. Girard, G. Lehnasch, & M. F. Shahab, 2008, 3D Unsteady Numerical Investigation of an Overexpanded Thrust Optimized Contour Nozzle. Sixth European Symposium on Aerothermodynamics for Space Vehicles, Versaille, France.

[19] S. Girard, H. Deniau, A; T. Nguyen & T. Alziary de Roquefort, 2001, Etude de l'écoulement dans une tuyére propulsive à contour parabolique en régime surdétendu. 37^{eme} Colloque d'Aérodynamique Appliquée de l'AAAF: Aérodynamique et Propulsion des Véhicules à grande vitesse., Aracachon, France.

[20] D. Lovely & R. Haimes, 1999, Shock detection function from computational fluid dynamics results. AIAA paper 99-3285.